PNAS
www.pnas.org

Supporting Information for

Thermodynamic Controls on Rates of Iron Oxide Reduction by Extracellular Electron Shuttles

Meret Aeppli, Sébastien Giroud, Sanja Vranic, Andreas Voegelin, Thomas B. Hofstetter* & Michael Sander*

***Corresponding authors: Thomas B. Hofstetter and Michael Sander.**
E-mail: thomas.hofstetter@eawag.ch, michael.sander@env.ethz.ch

This PDF file includes:

List of Figures

List of Tables

List of Sections

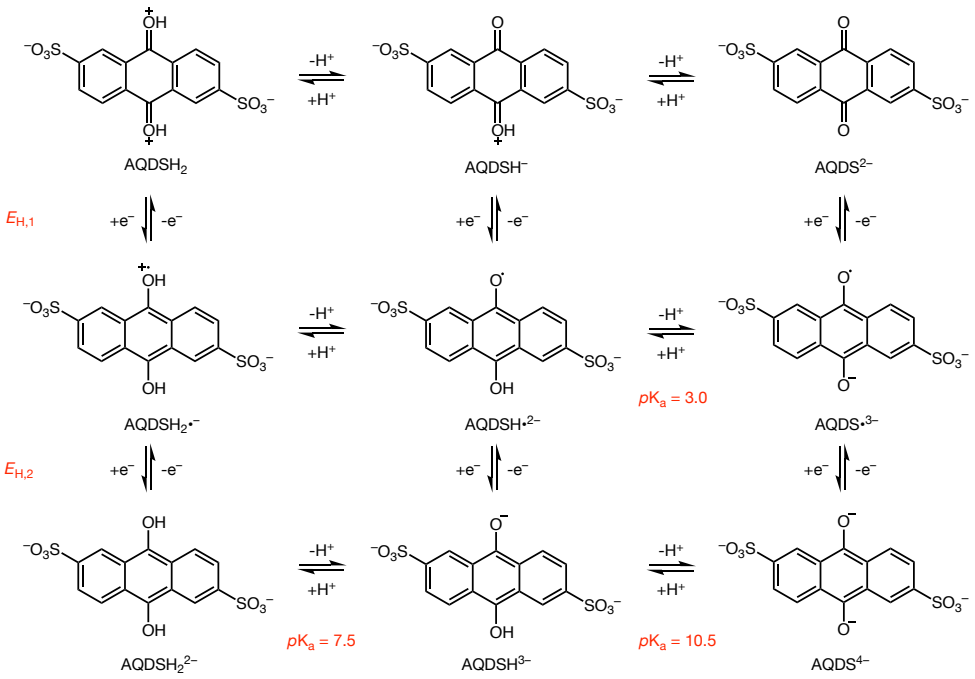

Figure S1. Nine-membered square scheme for the anthraquinone-2,6-disulfonate system. pK_a values[1] and reduction potentials for the first ($E_{H,1}$) and second electron transfer ($E_{H,2}$) during anthraquinone-2,6-disulfonate reduction are marked in red.

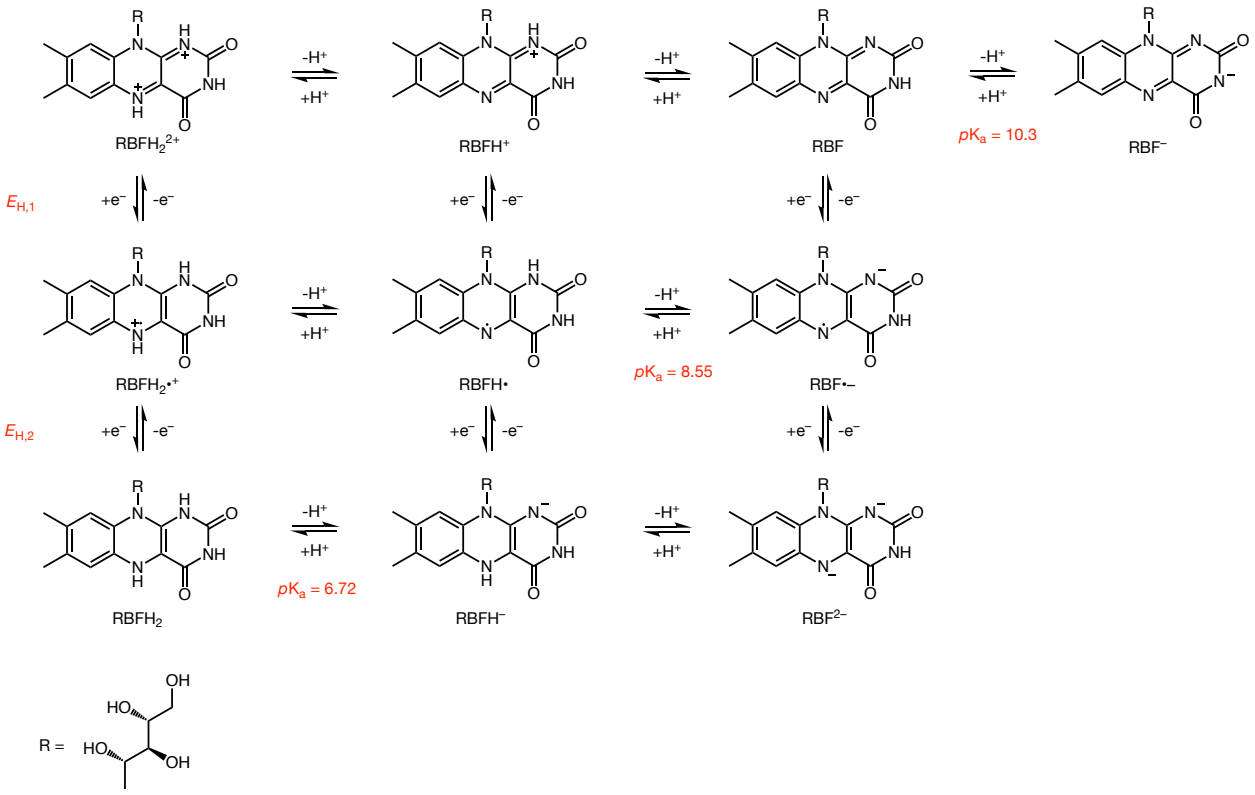

Figure S2. Nine-membered square scheme for the riboflavin (7,8-dimethyl-10-[(2S,3S,4R)-2,3,4,5-tetrahydroxypentyl]benzo[g]pteridine-2,4-dione) system. $p\mathrm{K}_a$ values[2] and reduction potentials for the first ($E_{\mathrm{H},1}$) and second electron transfer ($E_{\mathrm{H},2}$) during riboflavin reduction are marked in red.

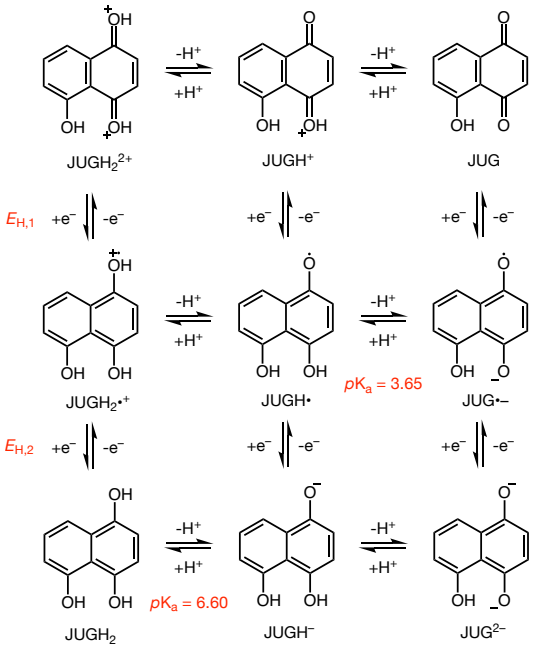

Figure S3. Nine-membered square scheme for the juglone (5-hydroxy-1,4-naphthalenedione) system. $p\mathrm{K}_a$ values[3,4] and reduction potentials for the first ($E_{\mathrm{H},\,1}$) and second electron transfer ($E_{\mathrm{H},\,2}$) during juglone reduction are marked in red.

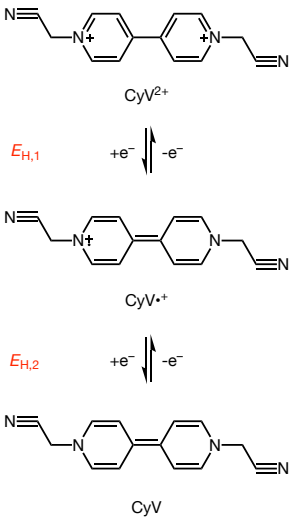

Figure S4. Electron transfers between the different redox species of cyanomethylviologen (1,1′-Bis(cyanomethyl)-4,4′-bibyridinium dibromide). Reduction potentials for the first ($E_{H,\,1}$) and second electron transfer ($E_{H,\,2}$) during cyanomethylviologen reduction are marked in red.

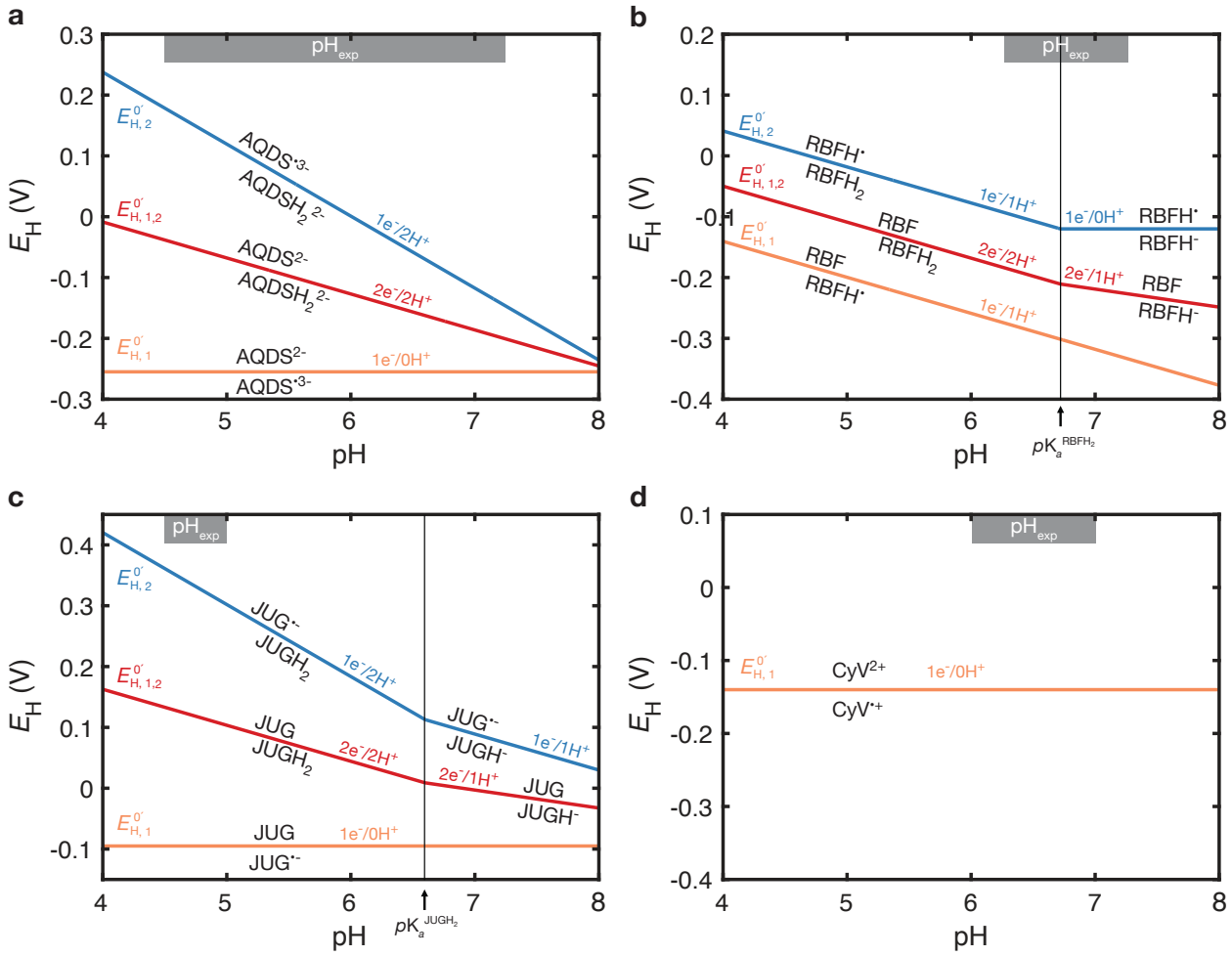

Figure S5. see next page

Figure S5 ***(previous page).*** E_{H}-pH diagrams for the two-electron extracellular electron shuttles (EES) (**a**) anthraquinone-2,6-disulfonate, (**b**) riboflavin, and (**c**) juglone and (**d**) the one-electron EES cyanomethylviologen. Colored lines represent reduction potentials of the quinone/hydroquinone ($E^{0'}_{\mathrm{H,\,1,2}}$, red), semiquinone/hydroquinone ($E^{0'}_{\mathrm{H,\,2}}$, blue) and quinone/semiquinone ($E^{0'}_{\mathrm{H,\,1}}$, orange) redox couples. The numbers of electrons (e^-) and protons (H^+) transferred in each reaction are noted on the lines. Diagrams for anthraquinone-2,6-disulfonate and riboflavin are replotted from Figure 1a,c and were drawn using published standard reduction potentials[5,6], and $p\mathrm{K}_a^{\mathrm{AQDSH}^{\bullet 2-}} = 3.0$[1] for anthraquinone-2,6-disulfonate semiquinone, $p\mathrm{K}_a^{\mathrm{RBFH}^{\bullet}} = 8.55$[5] for riboflavin semiquinone and $p\mathrm{K}_a^{\mathrm{RBFH_2}} = 6.72$[2] for reduced riboflavin. Diagrams for juglone and cyanomethylviologen were drawn using published standard reduction potentials[3,7,8] and $p\mathrm{K}_a^{\mathrm{JUGH}^{\bullet}} = 3.65$[3] for juglone semiquinone and $p\mathrm{K}_a^{\mathrm{JUGH_2}} = 6.60$[4] for reduced juglone.

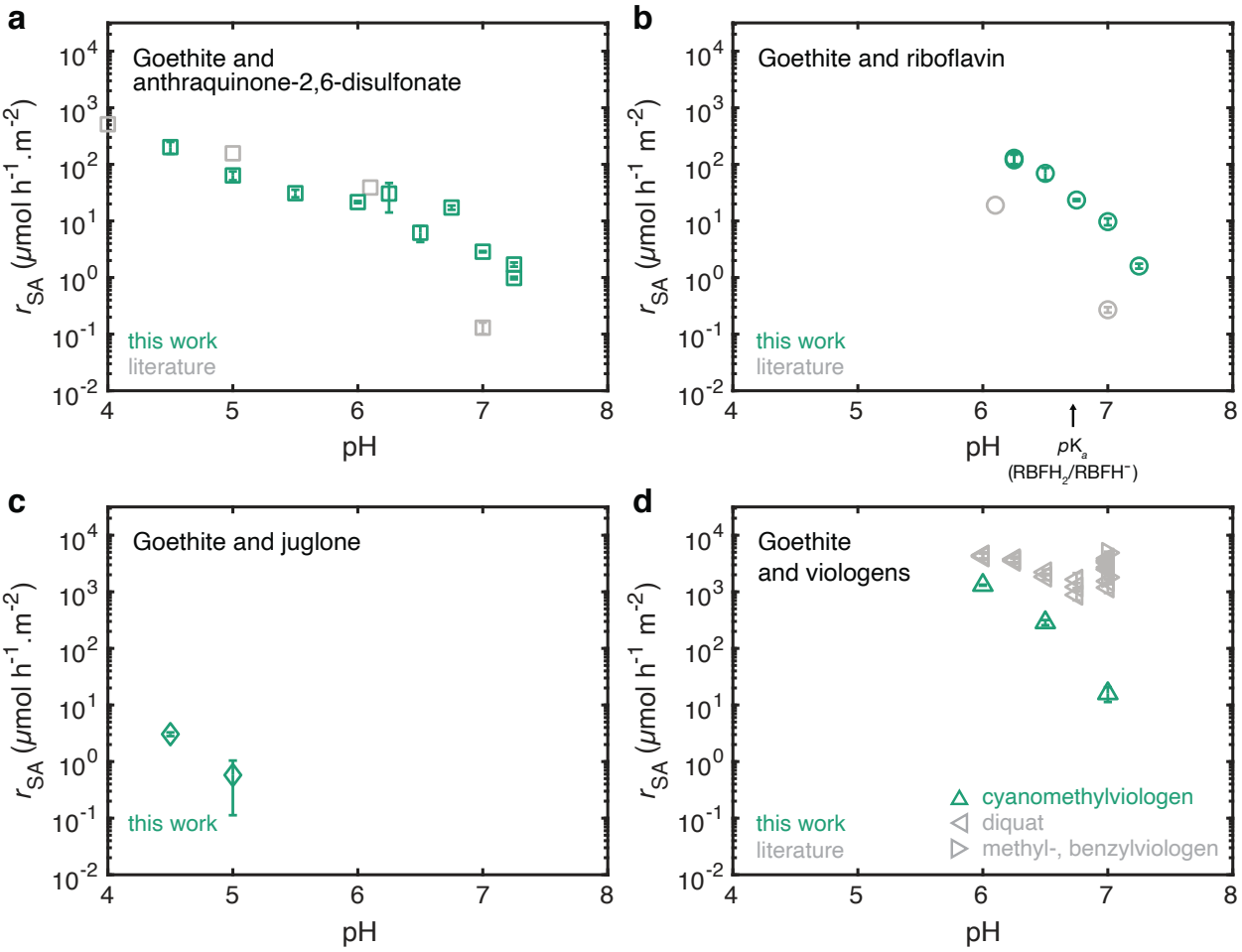

Figure S6. Surface area-normalized initial rates of goethite reduction, r_{SA}, by reduced (**a**) anthraquinone-2,6-disulfonate, (**b**) riboflavin, (**c**) juglone and (**d**) various viologens versus pH. r_{SA} values are re-plotted from Figures 2 and 3 with values measured herein shown in green and literature-reported values in gray[9–11].

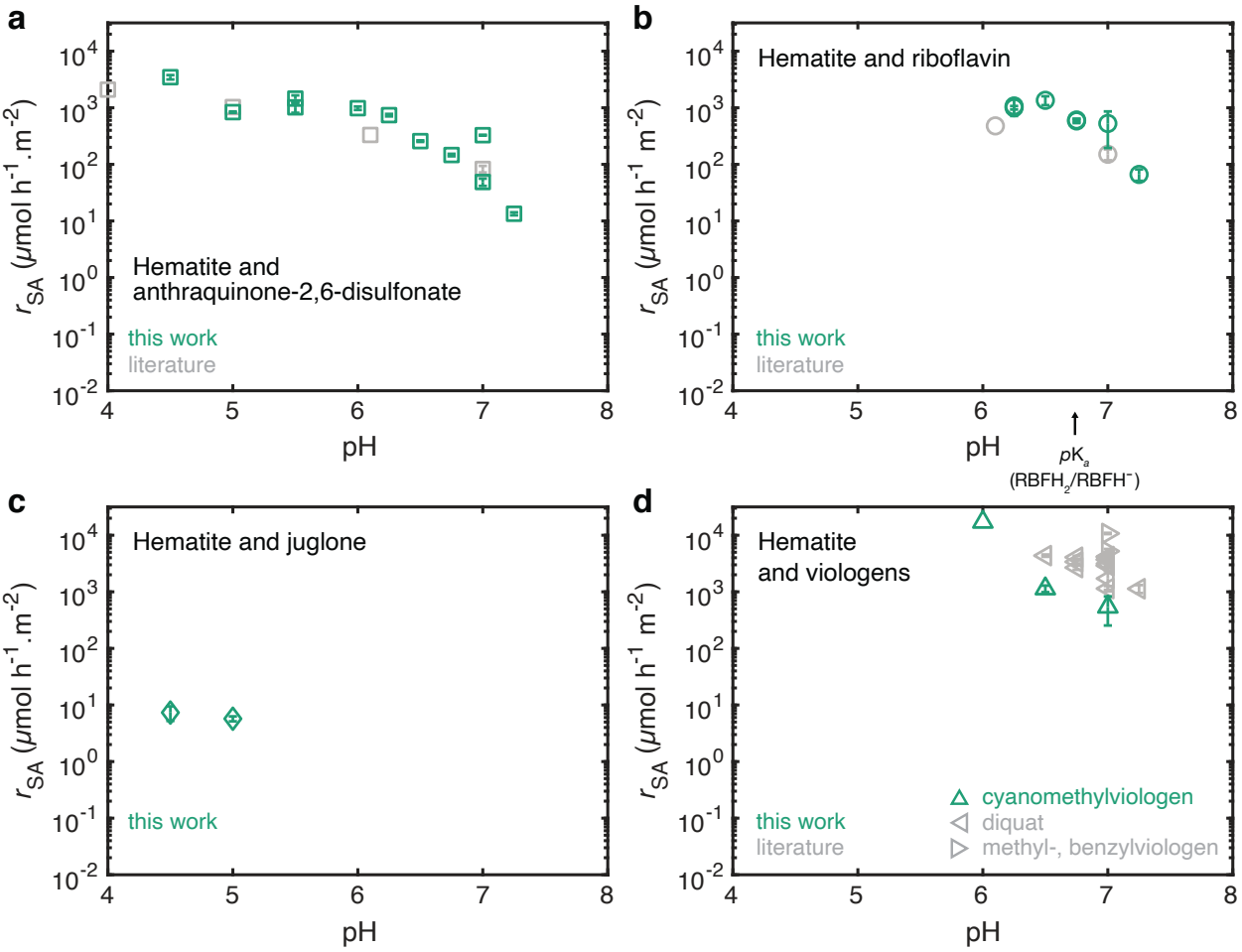

Figure S7. Surface area-normalized initial rates of hematite reduction, r_{SA}, by reduced (**a**) anthraquinone-2,6-disulfonate, (**b**) riboflavin, (**c**) juglone and (**d**) various viologens versus pH. r_{SA} values are re-plotted from Figures 2 and 3 in the main manuscript with values measured herein shown in green and literature-reported values in gray[9,10,12].

S1 Analysis of literature-reported rates of goethite and hematite reduction

We compiled rates of goethite and hematite reduction by various extracellular electron shuttles (EES) from the literature. The following paragraphs describe how we treated these rates and how we estimated the Gibbs free energies at which these rates were measured.

In our previous publication[9], we quantified reduction rates of the same goethite and hematite batches studied herein using mediated electrochemical reduction with diquat and cyanomethylviologen as electron transfer mediators. We used these rates and the $\Delta_r G$ values reported in that work without any additional data treatment.

Shi et al., 2013[10] determined rates of goethite and hematite reduction by reduced anthraquinone-2,6-disulfonate, riboflavin, and methyl- and benzylviologen using UV-vis spectroscopy (in experiments with viologens) in combination with the quantification of dissolved Fe(II) formation (in experiments with anthraquinone-2,6-disulfonate and riboflavin). The goethite used in that study was synthesized according to the same procedure as the goethite herein but the hematite was synthesized according to a different procedure[13]. The goethite and hematite in Shi et al. were of similar sizes and shapes as the ones used herein: goethite particles were acicular and had lengths of 200-500 nm and widths of 20-100 nm; hematite particles were spherical and had diameters of 30-50nm. Surface areas were 38 m^2 g^{-1} for goethite, 34 m^2 g^{-1} for hematite, as determined by N_2-BET. Shi et al. performed iron oxide reduction experiments at pH 4.0 to 7.0 with initial concentrations of 0.1 mM Fe(III) and 0.1 mM electron equivalents of reduced EES. Iron oxide reduction rates were determined from the first 10% portion of the reaction, i.e. using the same procedure as in herein.

We herein used these rates without further treatment. We calculated the respective $\Delta_r G^{0'}_{1,2}$ and $\Delta_r G^{0'}_{2}$ values as described above using a Fe^{2+} concentration of 0.01 mM (i.e., the concentration after the first 10% of the reaction), and E^0_H=−0.45 V for methylviologen[14] and E^0_H=−0.36 V for benzylviologen[14]. We note that the three goethite reduction rates that fall below the free energy relationship in Figure 3a in the main manuscript (goethite reduction by reduced riboflavin at pH 6.1 and 7.0 and anthrahydroquinone-2,6-disulfonate at pH 7.0) were determined as formation rates of dissolved Fe(II). This observation strongly suggests that formation rates of dissolved Fe(II) under these conditions were smaller than rates of electron transfer from the respective reduced EES to goethite.

Burgos et al., 2003[12] determined rates of hematite reduction by reduced anthraquinone-2,6-disulfonate using UV-vis spectroscopy. Hematite was purchased from J.T. Baker (Phillipsburg, NJ) and had a surface area of 9.04 m^2 g^{-1}, as determined by N_2-BET. Burgos et al. performed hematite reduction experiments at pH 6.8 and initial concentrations of 2 g L^{-1} hematite and 0.25 mM electron equivalents of reduced EES. We derived the rate of hematite reduction in these experiments according to the procedure in Shi et al.[10]. We calculated the respective $\Delta_r G^{0'}_{1,2}$ and $\Delta_r G^{0'}_{2}$ values as described above using a Fe^{2+} concentration of 0.025 mM (i.e., the concentration after the first 10% of the maximum reaction).

Ross et al., 2009[11] determined the second order rate constant of goethite reduction by reduced riboflavin using UV-vis spectroscopy. Goethite was synthesized according to Schwertmann and Cornell[13] and the resulting particles had a surface area of 34 m^2 g^{-1}, as determined by N_2-BET. Ross

et al. performed goethite reduction experiments at pH 7.0 and different of goethite concentrations. We derived a goethite reduction rate from the second order rate constant according to the procedure in Shi et al.[10]. We determined the corresponding $\Delta_r G_2$ value as described above for Shi et al.[10].

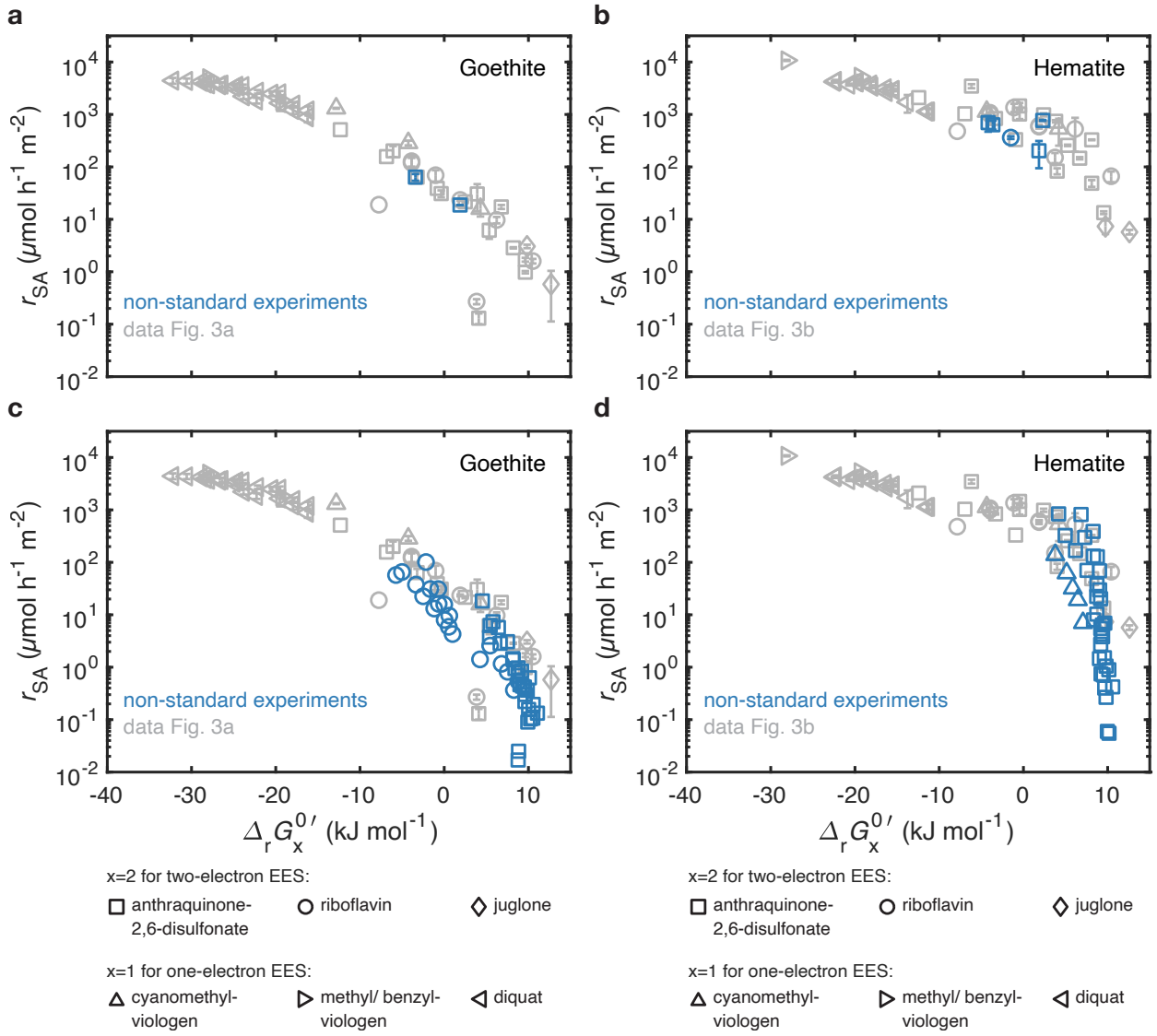

Figure S8. see next page

Figure S8 ***(previous page).*** Free energy relationships for goethite and hematite in manipulation experiments. Surface area-normalized initial reduction rates, r_{SA}, for goethite and hematite are shown versus the Gibbs free energy of the first electron transfer from two-electron reduced electron transfer shuttles (EES) to the iron oxides ($\Delta_r G_2^{0'}$) and versus the Gibbs free energy of the electron transfer from the semiquinone EES to the iron oxides for one-electron EES ($\Delta_r G_1^{0'}$). **a, b**, r_{SA} values measured in experiments at initial concentrations of oxidized EES species corresponding to 10% of the initial concentration of the reduced EES (blue symbols). **c, d**, Changes in r_{SA} values for goethite and hematite over the course of single experiments (blue symbols). Rates and Gibbs free energies were determined as described in Supporting Figure S9. Data from Figure 3a, b are re-plotted in gray for reference.

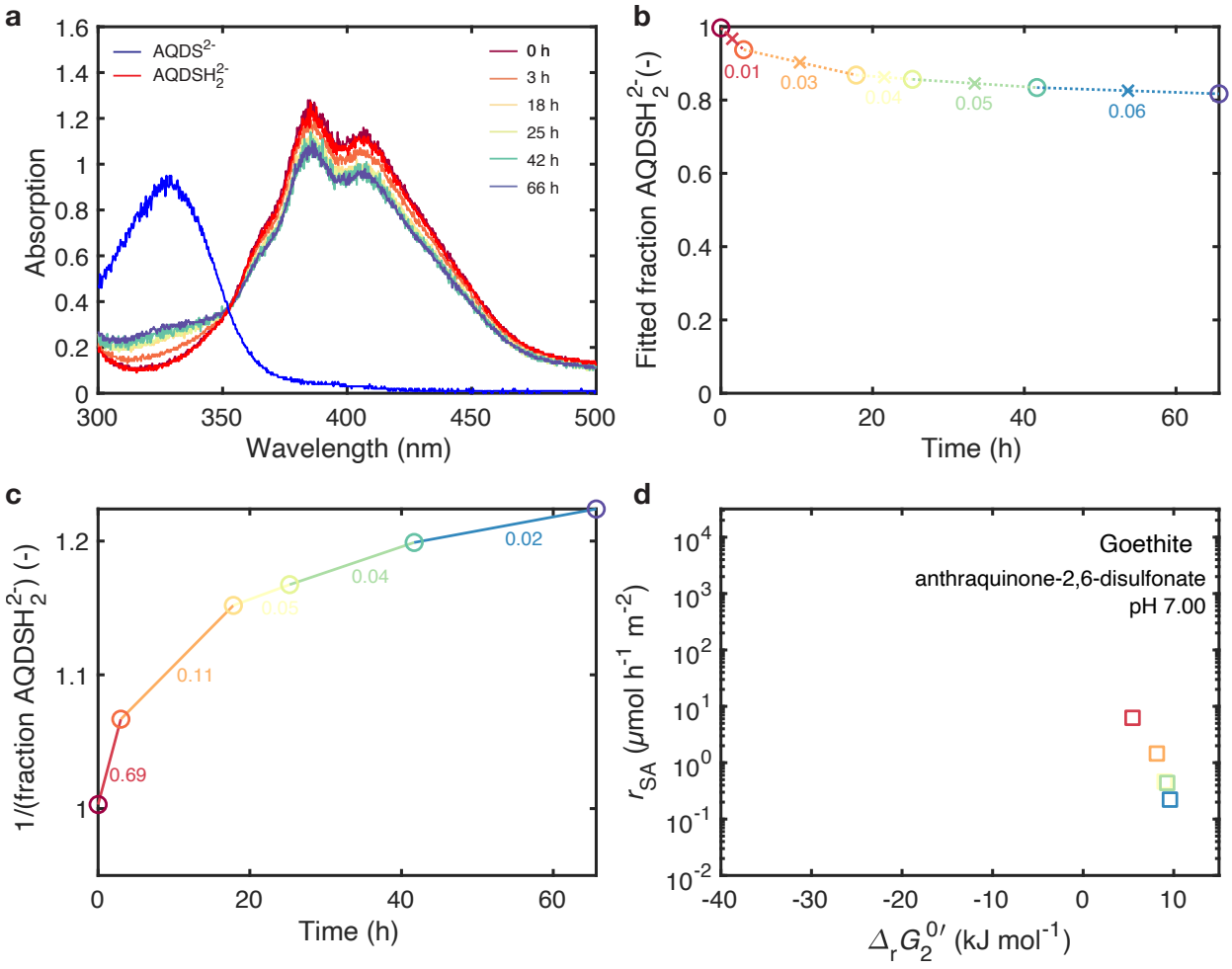

Figure S9. see next page

Figure S9 ***(previous page)*****.** Changes in iron oxide reduction rate and Gibbs free energy during an exemplary experiment with goethite and anthraquinone-2,6-disulfonate at pH 7.00. **a**, Absorption spectra of mixtures of oxidized ($AQDS^{2-}$) and reduced anthraquinone-2,6-disulfonate ($AQDSH_2^{2-}$) collected during the experiment. **b**, Changes in the fitted fraction of $AQDSH_2^{2-}$ during the experiment. The concentration of Fe(II) at the midpoint between two sampling points (marked by x) was used to calculate the Gibbs free energy of the first electron transfer from $AQDSH_2^{2-}$ to goethite, $\Delta_r G_2^{0'}$. The concentration values are given on the plot (in mM). **c**, Changes in the inverse of the fraction of $AQDSH_2^{2-}$ during the experiment. The slopes between sampling points (shown as colored lines) correspond to the observed rate constants, k_{obs}, following equation S3 and are given on the plot (in h^{-1}). **d**, Relationship between r_{SA} and $\Delta_r G_2^{0'}$ during the experiment. r_{SA} values were determined from k_{obs} values in panel c using equation S4. $\Delta_r G_2^{0'}$ were determined using equation S6 and Fe(II) concentrations in panel b. The color coding is the same as in panels a-c.

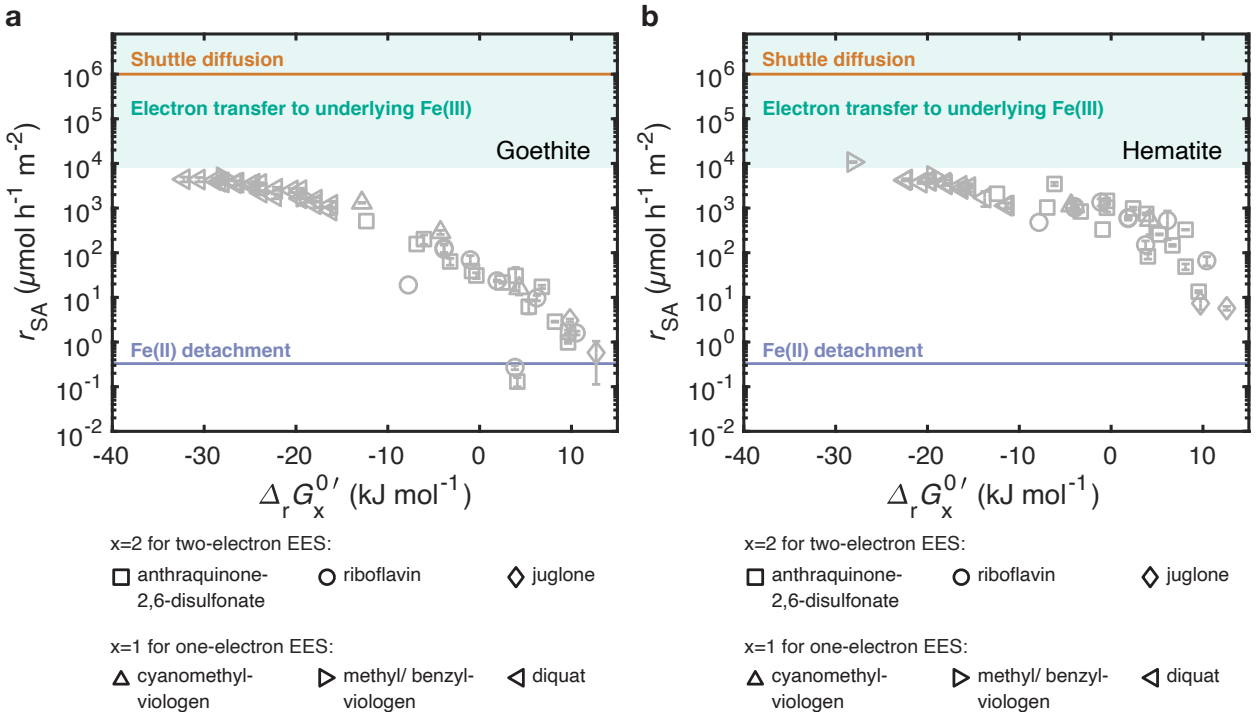

Figure S10. Kinetics of processes affecting iron oxide reduction rates. Initial surface area-normalized reduction rates, r_{SA}, of (**a**) goethite and (**b**) hematite with different EES are re-plotted in gray from Figure 3a, b versus the Gibbs free energy of the first electron transfer from two-electron reduced electron transfer shuttles (EES) to the iron oxides ($\Delta_r G_2^{0\prime}$) and versus the Gibbs free energy of the electron transfer from the semiquinone EES to the iron oxides for one-electron EES ($\Delta_r G_1^{0\prime}$). Rates of EES diffusion (orange) were estimated according to the procedure in Figure 5 in Glasser et al., 2017[15] using the diffusion coefficients for pyocyanin therein and assuming spherical iron oxide particles with diameters of 30 nm. The range of electron transfer rates from Fe(II) complexes on oxide surfaces to underlying Fe(III) (green) were obtained by Zarzycki et al., 2015[16] in stochastic simulations of atom exchange in Fe(II)-catalyzed recrystallization of goethite. Using the same method, Zarzycki et al., 2015[16] determined rates of Fe(II) detachment from goethite surfaces (blue).

S2 Chemicals

7,8-dimethyl-10-[(2S,3S,4R)-2,3,4,5-tetrahydroxypentyl]benzo[g]pteridine-2,4-dione (riboflavin) was purchased from Sigma. 3-(*N*-Morpholino) propanesulfonic acid (MOPS), acetic acid, and anthraquinone-2,6-disulfonate were purchased from Sigma-Aldrich. 5-hydroxy-1,4-naphthalenedione (juglone) was purchased from Aldrich. 2-(*N*-Morpholino) ethanesulfonic acid (MES) was purchased from Merck. 1,1′-Bis(cyanomethyl)-4,4′-bibyridinium dibromide (cyano- methylviologen) was synthesized and re-crystallized as described previously[7,17].

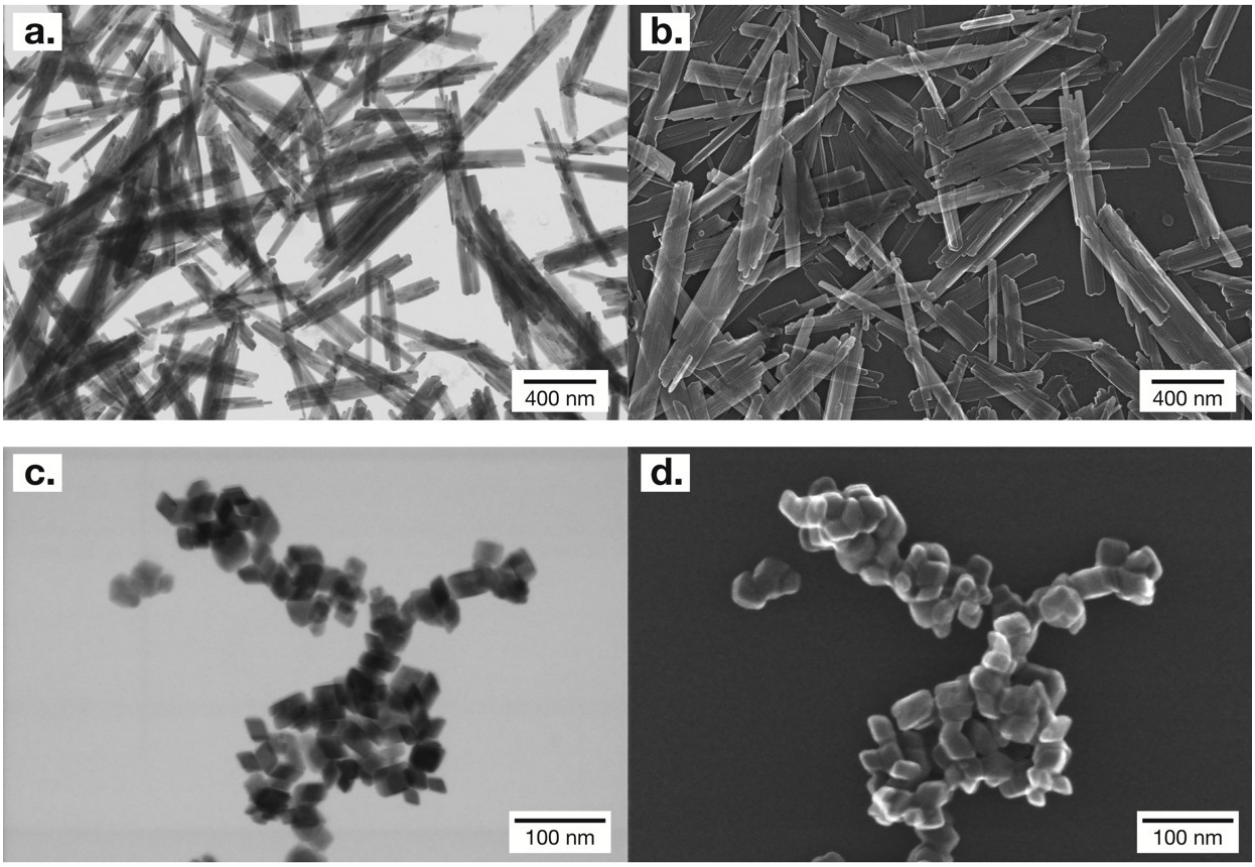

Figure S11. Electron microscopy images of goethite (**a**, **b**) and hematite (**c**, **d**). Particles were deposited onto grids coated with a holey carbon support film and analyzed using a scanning transmission electron microscope (2700Cs, Hitachi) operated at an acceleration voltage of 200 kV. For image acquisition, bright field (panels a, c) and secondary electron (panels b, d) detectors were used. Goethite particles were acicular with lengths of around 1 μm and widths of around 100 nm. Hematite particles were diamond-shaped with diameters of around 30 nm.

S3 Matlab code for deconvolution of absorption spectra

Absorption spectra were deconvoluted using the Spectr-O-Matic toolbox[18] in Matlab (MathWorks) according to the following code.

```
%% import data
spec_ref=specdata.load('ref.txt'); % reference spectra red and ox
spec_sample=specdata.load('GOE_A.txt'); % sample spectra
%% User input
t_vec=[0;25;65.16;134;270;1146.25;2000;4000]; % time vector
Nspec=length(t_vec); % number of spectra
wl_min=300; wl_max=500; % min and max wavelengths
spec_ref = spec_ref.setxlim([wl_min wl_max]);
spec_sample = spec_sample.setxlim([wl_min wl_max]);
%% Plot raw data and decompose
figure(001); set(001,'units','normalized','outerposition',[0 0 1 1])
subplot(2,2,1)
hold on
frac=zeros(Nspec,2); F=specdata(1,Nspec);
for i=1:Nspec;
    plot(spec_sample(i))
    c=spec_ref\spec_sample(i);
    for j=1:2
        frac(i,j)=c(j);
    end
```

```
21      F(i)=sum(spec_ref*frac(i,1:2));
22      R(i)=F(i)-spec_sample(i);
23      legendInfo{i} = ['spec' num2str(i)];
24  end
25  plot(spec_ref(1),'b'); plot(spec_ref(2),'r')
26  text(0.05,0.98,'ref_{red}','color',[0 0 1],'units','normalized')
27  text(0.05,0.9,'ref_{ox}','color',[1 0 0],'units','normalized')
28  legend(legendInfo)
29  ylabel('Absorption');xlabel('Wavelength (nm)');box on
30  %% Plot fits
31  set(0,'DefaultAxesColorOrder',cbrewer('qual','Set1',3))
32  figure(002);set(002,'units','normalized','outerposition',[0 0 1 1])
33  for i=1:Nspec
34      subplot(2,4,i)
35      hold on
36      plot(spec_sample(i),F(i),R(i))
37      legend('measured','fit','residual','location','south')
38      xlim([300 500])
39      ylim([-0.5 1.5])
40      txt_red={['f_{red}=',num2str(frac(i,1)/(frac(i,1)+frac(i,2)),3)]};
41      txt_ox={['f_{ox}=',num2str(frac(i,2)/(frac(i,1)+frac(i,2)),3)]};
42      text(0.05,0.95,txt_red,'color','k','units','normalized')
43      text(0.05,0.88,txt_ox,'color','k','units','normalized')
44      box on
45  end
46  %% Plot 2nd order fit
```

```
figure(001)
subplot(2,2,2)
hold on
for i=1:Nspec;
    plot(t_vec(i),1/(frac(i,1)/(frac(i,1)+frac(i,2))));
end
vec_fit=[1:4]; t_vec_fit=t_vec(vec_fit);
frac_red=1./(frac(vec_fit,1)./(frac(vec_fit,1)+frac(vec_fit,2)));
x=t_vec_fit;y=frac_red;
[data_x, data_y_f] = prepareCurveData( x, y );
ft = fittype( 'm*x+1', 'independent', 'x', 'dependent', 'y' );
opts = fitoptions( 'Method', 'NonlinearLeastSquares' );opts.Display = ...
    'Off';opts.StartPoint = [0.001];
[fitresult, gof] = fit( data_x, data_y_f, ft, opts );
coeff=coeffvalues(fitresult);coeff_slope=coeff(1);
t_vec_plot=[t_vec(1):0.1:t_vec(4)];
plot(t_vec_plot,coeff_slope*t_vec_plot+1,'-','linewidth',1.5,'color',[0 ...
    0.447 0.741])
txt_fit={['linear fit \it k\rm=',num2str(coeff_slope),'min^{-1}']};
text(0.95,0.95,txt_fit,'color','k','units','normalized')
xlabel('Time (min)');ylabel('1/frac_{red} (-)');box on
```

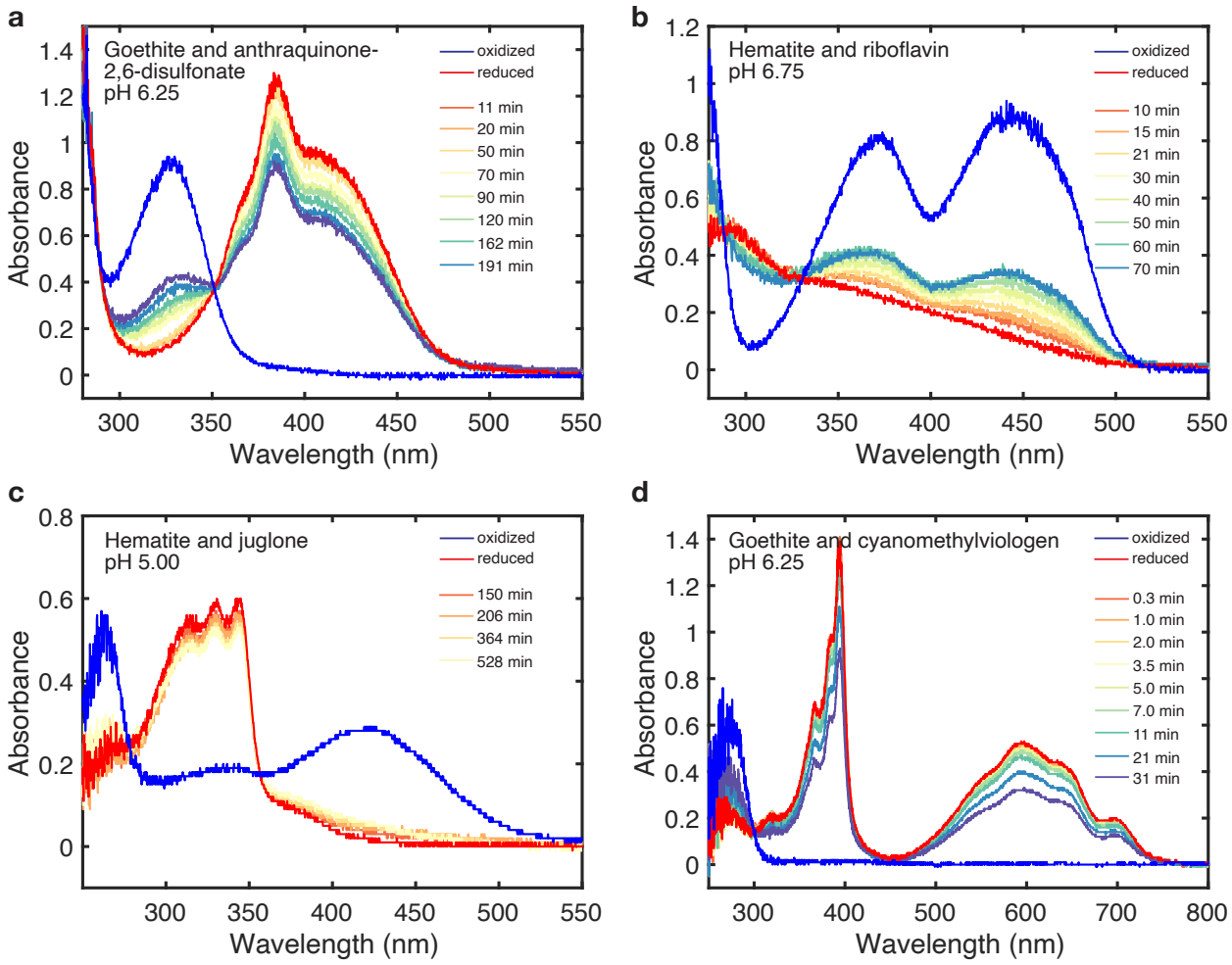

Figure S12. Absorption spectra of extracellular electron shuttles (EES) collected during exemplary iron oxide reduction experiments with (**a**) anthraquinone-2,6-disulfonate (goethite at pH 6.25), (**b**) riboflavin (hematite at pH 6.75), (**c**) juglone (hematite at pH 5.00), and (**d**) cyanomethylviologen (goethite at pH 6.25). Reference spectra of the fully reduced and oxidized EES species are shown in blue and red, respectively. Experiments were performed as described in the Materials and Methods section.

S4 Kinetic analysis

We determined initial rates of goethite and hematite reduction, r_0 [M h^{-1}], assuming a second order rate law (equation S1). We calculated initial rates for the first 10% of the complete redox reaction, i.e. until 10% of the added reduced EES were oxidized.

$$r_0 = -\frac{d[Fe^{III}]}{dt} = -\frac{d[shuttle^{red}]}{dt} = \frac{d[shuttle^{ox}]}{dt} = k \cdot [shuttle_{red}]^{\alpha} \cdot [Fe^{III}]^{\beta} \quad \text{(S1)}$$

where k is the second order rate constant [M^{-1} h^{-1}], [$shuttle_{red}$] and [$shuttle_{ox}$] are the concentrations of hydroquinone and quinone species of the EES, respectively, in electron equivalents, and [Fe(III)] is the concentration of Fe(III) in the oxide. In all experiments, [$shuttle_{red}$]=[Fe(III)] at all times t. Under the assumption that the reaction is first order with respect to [$shuttle_{red}$] and [Fe(III)](i.e., α=β=1), equation S1 integrates to equation S2.

$$\frac{1}{shuttle_{red}} = \frac{1}{[shuttle_{red,0}]} + k \cdot t \quad \text{(S2)}$$

where [$shuttle_{red,\,0}$] is the initial concentration of reduced EES. The concentration of reduced EES at each time t equals the fraction of total EES that was reduced at time t multiplied by the initial concentration of reduced EES, i.e., [$shuttle_{red}$]=f_{red}·[$shuttle_{red,\,0}$]. Substituting this expression into equation S2 and multiplying by [$shuttle_{red,\,0}$] yields equation S3.

$$\frac{1}{f_{red}} = 1 + k \cdot [shuttle_{red,0}] \cdot t = 1 + k_{obs} \cdot t \quad \text{(S3)}$$

We obtained k_{obs} [h^{-1}] from a linear fit of equation S3 to $1/f_{red}$ versus t. An exemplary fit is shown in Figure S13c. We normalized r_0 to the initial iron oxide surface area to obtain r_{SA} [mol m^{-2} h^{-1}]

using equation S4 .

$$r_{SA} = \frac{k \cdot [\text{shuttle}_{red,0}] \cdot [Fe_0^{III}]}{SA \cdot M_w \cdot [\text{shuttle}_{red,0}]}$$

$$= \frac{k \cdot [\text{shuttle}_{red,0}]^2}{SA \cdot M_w \cdot [\text{shuttle}_{red,0}]}$$

$$= \frac{k \cdot [\text{shuttle}_{red,0}]}{SA \cdot M_w} = \frac{k_{obs}}{SA \cdot M_w} \quad \text{(S4)}$$

where SA is the surface area of the iron oxide (36 m^2g^{-1} for goethite and 46 m^2g^{-1} for hematite), and M_w is the molar mass of goethite and hematite per Fe(III) (88.85 g $mol^{-1}_{Fe^{III}}$ for goethite, α-FeOOH, and 79.85 g $mol^{-1}_{Fe^{III}}$ for hematite, α-Fe_2O_3).

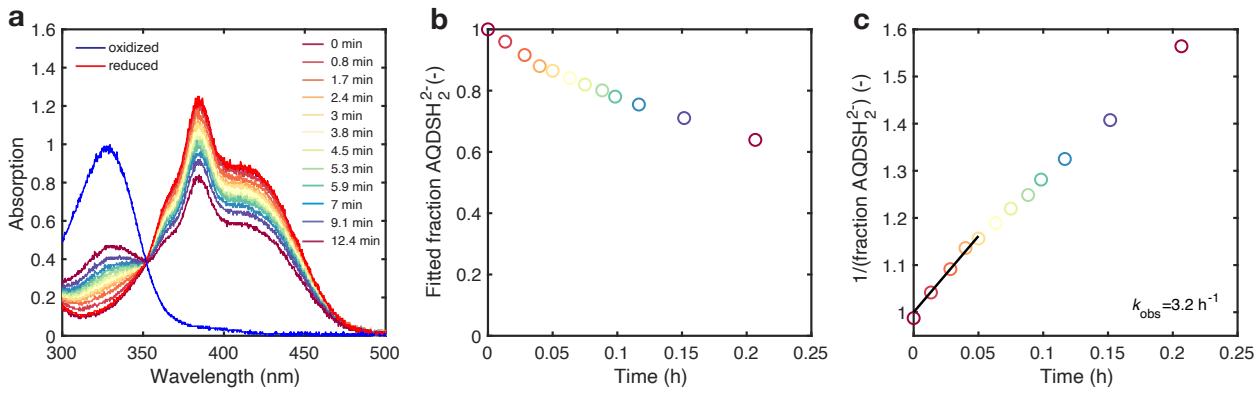

Figure S13. Example for the determination of hematite reduction rates by reduced anthraquinone-2,6-disulfonate at pH 5.00 (initial concentrations: 0.32 mM hematite-Fe(III) and 0.16 mM reduced anthraquinone-2,6-disulfonate). (**a**) Absorbance spectra of anthraquinone-2,6-disulfonate were collected at multiple time points during the experiment. (**b**) Changes in the fraction of reduced anthraquinone-2,6-disulfonate ($AQDSH_2^{2-}$) over the course of the experiment were determined from deconvolution of the spectra in panel a as described in the Materials and Methods section. (**c**) The observed rate constant for hematite reduction, k_{obs} [h^{-1}], was determined from a linear fit of equation S3 to 1/(fraction $AQDSH_2^{2-}$) versus time.

S5 Thermodynamic calculations

Terminology. We follow the IUPAC convention of writing the reduction/oxidation potential of a compound in the reductive direction. All potentials are referenced to the standard hydrogen electrode (indicated by the subscript $_{H}$). Standard reduction potentials (i.e., equal activity of all species) are depicted by the superscript ^{0}. Reduction potentials that are corrected for H^+ activity (but for which equal activities of all other species are assumed) are depicted by the superscript $^{0'}$. The subscript $_{1,2}$ refers to the average two-electron transfer of the electron transfer shuttle (EES), and the subscripts $_1$ and $_2$ refer to the first and second electron, respectively, transferred during the reduction of the EES.

Calculation of Gibbs free energies. We calculated the Gibbs free energy, $\Delta_r G_x^{0'}$ [kJ mol^{-1} electrons transferred], for the reductive dissolution of goethite and hematite by reduced EES according to equation S6 (equivalent to equation 19 in the main manuscript). The subscript $_x$ refers to the first (x=1) and second (x=2) electron transfer during the reduction of the EES and the averaged two-electron transfer (x=1,2).

$$\Delta_r G_x^{0'} = -n \cdot F \cdot \left(E_H(\text{oxide}) - E_{H,\,x}\right) \tag{S5}$$

$$\Delta_r G_x^{0'} = -n \cdot F \cdot \left(E_H^0(\text{oxide}) - \frac{2.303 \cdot R \cdot T}{F} \cdot \left(\log(\{Fe_{aq}^{2+}\}) + 3\text{pH}\right) - E_{H,\,x}^{0'}\right) \tag{S6}$$

where n is the number of electrons transferred in the reaction (n = 1 for the reduction of ferric to ferrous iron), F is the Faraday constant, E_H(oxide) and $E_{H,\,x}$ are the reduction potentials of the iron oxide and the EES at experimental pH and ferrous iron concentration, E_H^0(oxide) is the standard reduction potential of the iron oxide (E_H^0(oxide)=0.768 V [19] and 0.769 V [19] for goethite and hematite,

respectively), R is the gas constant, T is the absolute temperature, and $\{Fe^{2+}_{aq}\}$ is the activity of dissolved Fe^{2+} (calculated as the product of an activity coefficient of 0.785 and the concentration of dissolved Fe^{2+} [9]).

We calculated $E^{0}_{H,\,x}$ values for the i) quinone/hydroquinone (x=1,2; average two-electron reduction potential), ii) quinone/semiquinone (x=1; reduction potential at which the second electron is transferred from the semiquinone to the second Fe(III) atom), and iii) the semiquinone/hydroquinone (x=2; reduction potential at which the first electron is transferred from the hydroquinone to the first Fe(III) atom) redox couple of the EES. Table S1 lists $E^{0'}_{H,\,1,2}$ and $E^{0'}_{H,\,1}$ values from the literature. We used these values to calculate $E^{0'}_{H,\,2}$ (given that $E^{0'}_{H,\,1,2}$ is the average of $E^{0'}_{H,\,1}$ and $E^{0'}_{H,\,2}$). We calculated all $E^{0'}_{H,\,x}$ values using the experimental proton activity and assumed equal activities of the hydroquinone, quinone and semiquinone species of the EES. This assumption was necessary because we could not experimentally quantify the concentrations of semiquinone EES. In the following, the procedures for calculating $E^{0}_{H,\,x}$ values are presented for each EES.

Table S1. Experimental reduction potentials of the quinone/hydroquinone ($E^{0'}_{H,\,1,2}$) and quinone/semiquinone ($E^{0'}_{H,\,1}$) redox couples of two-electron EES used to calculate Gibbs free energy values in this work. Experimental $E^{0'}_{H,\,1,2}$ and $E^{0'}_{H,\,1}$ values were compiled from the literature and used to calculate reduction potentials of the quinone/semiquinone redox couples ($E^{0'}_{H,\,1}$), as described in the text. For comparison, calculated $E^{0'}_{H,\,x}$) values from the literature are reported (where available).

Two-electron EES	$E^{0'}_{H,\,1,2}$ (V) experimental	$E^{0'}_{H,\,1}$ (V) experimental	$E^{0'}_{H,\,x}$ (V) calculated
Anthraquinone-2,6-disulfonate	0.228[20] (pH 0.00)	-0.255[1] (pH 7.00)	0.253[21] (x=1,2; pH 0.00)
Riboflavin	-0.219[22] (pH 7.00)	-0.318[6] (pH 7.00)	-0.313[5] (x=1; pH 7.00)
Juglone	-0.003[23] (pH 7.00)	-0.095[3] (pH 7.00)	-0.093[3] (x=1; pH 7.00)
Viologen		-0.14[7]	

Anthraquinone-2,6-disulfonate: The pH-dependencies of the reduction potentials for the anthraquinone-2,6-disulfonate system are illustrated in the Supporting Figure S5a and the corresponding molecular structures in Supporting Figure S1. In the pH range investigated herein (i.e., 4.50 to 7.25), $E^{0'}_{\mathrm{H},\,1,2}$ decreases by 0.059 V pH^{-1} with increasing pH[24] (equation S7).

$$E^{0'}_{\mathrm{H},\,1,2} = E^{0}_{\mathrm{H},\,1,2} - \frac{2.303 \cdot R \cdot T}{F} \cdot \mathrm{pH} \tag{S7}$$

where $E^{0}_{\mathrm{H},\,1,2}$=0.228 V[20]. We calculated $E^{0'}_{\mathrm{H},\,1}$ and $E^{0'}_{\mathrm{H},\,2}$ according to equations S8 and S9[24] (i.e., in the pH range 4.50 to 7.25 investigated herein, $E^{0'}_{\mathrm{H},\,1}$ is constant and $E^{0'}_{\mathrm{H},\,2}$ decreases by 0.118 V pH^{-1} with increasing pH).

$$E^{0'}_{\mathrm{H},\,1} = E^{0\ \mathrm{pH}\ 7.00}_{\mathrm{H},\,1} \tag{S8}$$

$$E^{0'}_{\mathrm{H},\,2} = 2 \cdot E^{0'}_{\mathrm{H},\,1,2} - E^{0'}_{\mathrm{H},\,1} \tag{S9}$$

where $E^{0\ \mathrm{pH}\ 7.00}_{\mathrm{H},\,1}$=−0.255[1].

Riboflavin: The pH-dependencies of the reduction potentials for the riboflavin system are illustrated in Supporting Figure S5b and the corresponding molecular structures in Supporting Figure S2. These dependencies were reported for flavin mononucleotide but are equivalent to those of riboflavin[5,6,20,25]. In the pH range investigated herein (i.e., 6.25 to 7.25), $E^{0'}_{\mathrm{H},\,1,2}$ decreases by 0.059 V pH^{-1} with increasing pH≤$p\mathrm{K}_a^{\mathrm{RBFH_2}}$ = 6.72[2] of reduced riboflavin (equation S10) and by 0.030 V above this pH (equation S11).

$$E^{0'}_{\mathrm{H},\,1,2} = E^{0\ \mathrm{pH}\ 6.72}_{\mathrm{H},\,1,2} - \frac{2.303 \cdot R \cdot T}{F} \cdot (\mathrm{pH\text{-}6.72})\ (\mathrm{at\ pH} \leq\ \mathrm{pH}\ 6.72) \tag{S10}$$

$$E^{0'}_{\mathrm{H},\,1,2} = E^{0\ \mathrm{pH}\ 6.72}_{\mathrm{H},\,1,2} - \frac{2.303 \cdot R \cdot T}{2F} \cdot (\mathrm{pH\text{-}6.72})\ (\mathrm{at\ pH} > \mathrm{pH}\ 6.72) \tag{S11}$$

where $E^{0\,\mathrm{pH}\,6.72}_{\mathrm{H},\,1,2}$ was calculated from $E^{0\,\mathrm{pH}\,7}_{\mathrm{H},\,1,2}$=−0.219 V[22] using a slope of 0.030 V pH^{-1}. We calculated $E^{0'}_{\mathrm{H},\,1}$ and $E^{0'}_{\mathrm{H},\,2}$ according to equations S12 and S13 (i.e., $E^{0'}_{\mathrm{H},\,1}$ decreases by 0.059 V pH^{-1} with increasing pH from 6.25 to 7.25 and $E^{0'}_{\mathrm{H},\,2}$ decreases by 0.059 V pH^{-1} with increasing pH ≤ 7.00 and is pH-independent above this pH[5]).

$$E^{0'}_{\mathrm{H},\,1} = E^{0'\mathrm{pH}\,7}_{\mathrm{H},\,1} - \frac{2.303 \cdot R \cdot T}{F} \cdot (\mathrm{pH\text{-}7.00}) \tag{S12}$$

$$E^{0'}_{\mathrm{H},\,2} = 2 \cdot E^{0'}_{\mathrm{H},\,1,2} - E^{0'}_{\mathrm{H},\,1} \tag{S13}$$

where $E^{0'\mathrm{pH}\,7}_{\mathrm{H},\,1}$=−0.318 V[6].

Juglone: The pH-dependencies of the reduction potentials for the juglone systems are illustrated in Supporting Figure S5c and the corresponding molecular structures in Supporting Figure S3. In the pH range investigated herein (i.e., pH 4.50 to 5.00), $E^{0'}_{\mathrm{H},\,1,2}$ decreases by 0.059 V pH^{-1} with increasing pH at pH ≤ $p\mathrm{K}_a$ of 6.60 of the hydroquinone species[4] (equation S14) and by 0.030 V pH^{-1} above this pH[3,8] (equation S15).

$$E_{\mathrm{H},\,1,2} = E^{0'\mathrm{pH}\,6.60}_{\mathrm{H},\,1,2} - \frac{2.303 \cdot R \cdot T}{F} \cdot (\mathrm{pH\text{-}6.60})\ (\mathrm{at\ pH} \leq 6.60) \tag{S14}$$

$$E_{\mathrm{H},\,1,2} = E^{0'\mathrm{pH}\,6.60}_{\mathrm{H},\,1,2} - \frac{2.303 \cdot R \cdot T}{2F} \cdot (\mathrm{pH\text{-}6.60})\ (\mathrm{at\ pH} > 6.60) \tag{S15}$$

where $E^{0'\mathrm{pH}\,6.60}_{\mathrm{H},\,1,2}$ was calculated from $E^{0'\mathrm{pH}\,7}_{\mathrm{H},\,1,2}$=−0.003 V[23] using a slope of 0.030 V pH^{-1}. We calculated $E^{0'}_{\mathrm{H},\,1}$ and $E^{0'}_{\mathrm{H},\,2}$ according to equations S16 and S17[3,8] (i.e., in the pH range 4.50 to 5.00 investigated herein, $E^{0'}_{\mathrm{H},\,1}$ is pH-independent and $E^{0'}_{\mathrm{H},\,2}$ decreases by 0.118 V pH^{-1} with increasing pH).

$$E^{0'}_{\mathrm{H},\,1} = E^{0'\mathrm{pH}\,7}_{\mathrm{H},\,1} \tag{S16}$$

$$E^{0'}_{\mathrm{H},\,2} = 2 \cdot E^{0'}_{\mathrm{H},\,1,2} - E^{0'}_{\mathrm{H},\,1} \tag{S17}$$

where $E_{H,\,1}^{0'pH\,7}$=−0.093 V[3].

Cyanomethylviologen: Cyanomethylviologen undergoes pH-independent electron transfer reactions, as illustrated in Supporting Figure S5d (corresponding molecular structures in Supporting Figure S4). Viologen compounds have stable semiquinone species because the first electron transfer to the compound during its reduction occurs at higher reduction potentials than the second, i.e., $E_{H,1} > E_{H,2}$. In our experiments, we used the semiquinone species of cyanomethylviologen as reductant for goethite and hematite. Therefore, only $E_{H,\,1}^{0'}$ was relevant for our experiments which was calculated according to S18.

$$E_{H,\,1}^{0'} = E_{H}^{0} \tag{S18}$$

where E_{H}^{0}=−0.14 V for cyanomethylviologen[7].

References

1. Pal, H., Palit, D. K., Mukherjee, T. & Mittal, J. P. One-electron reduction of anthraquinone sulphonates: A pulse radiolysis study. *Int. J. Radiat. Appl. Instrum. C Radiat. Phys. Chem.* **37**, 227–235 (1991).

2. Draper, R. D. & Ingraham, L. L. A potentiometric study of the flavin semiquinone equilibrium. *Arch. Biochem. Biophys.* **125**, 802–808 (1968).

3. Mukherjee, T. One-electron reduction of juglone (5-hydroxy-1,4-naphthoquinone): A pulse radiolysis study. *Int. J. Radiat. Appl. Instrum. C Radiat. Phys. Chem.* **29**, 455–462 (1987).

4. Friedheim, E. A. Natural reversible oxidation-reduction systems as accessory catalysts in respiration: juglon and lawson. *Biochem. J.* **28**, 180–188 (1934).

5. Mayhew, S. G. The effects of pH and semiquinone formation on the oxidation-reduction potentials of flavin mononucleotide. A reappraisal. *Eur. J. Biochem.* **265**, 698–702 (1999).

6. Anderson, R. F. Energetics of the one-electron reduction steps of riboflavin, FMN and FAD to their fully reduced forms. *Biochim. Biophys. Acta Bioenergetics* **722**, 158–162 (1983).

7. Gorski, C. A., Kluepfel, L. E., Voegelin, A., Sander, M. & Hofstetter, T. B. Redox Properties of Structural Fe in Clay Minerals. 2. Electrochemical and Spectroscopic Characterization of Electron Transfer Irreversibility in Ferruginous Smectite, SWa-1. *Environ. Sci. Technol.* **46**, 9369–9377 (2012).

8. Grundl, T. J., Haderlein, S. B., Nurmi, J. T. & Tratnyek, P. G. Introduction to Aquatic Redox Chemistry. In Tratnyek, P. G., Grundl, T. J. & Haderlein, S. B. (eds.) *Aquatic Redox Chemistry* (American Chemical Society, Washington, DC, 2011).

9. Aeppli, M., Voegelin, A., Gorski, C. A., Hofstetter, T. B. & Sander, M. Mediated electrochemical reduction of iron (oxyhydr-)oxides under defined thermodynamic boundary conditions. *Environ. Sci. Technol.* **52**, 560–570 (2018).

10. Shi, Z., Zachara, J. M., Wang, Z., Shi, L. & Fredrickson, J. K. Reductive dissolution of goethite and hematite by reduced flavins. *Geochim. Cosmochim. Acta* **121**, 139–154 (2013).

11. Ross, D. E., Brantley, S. L. & Tien, M. Kinetic characterization of OmcA and MtrC, terminal reductases involved in respiratory electron transfer for dissimilatory iron reduction in *Shewanella oneidensis* MR-1. *Appl. Environ. Microbiol.* **75**, 5218–5226 (2009).

12. Burgos, W. D. *et al.* Reaction-based modeling of quinone-mediated bacterial iron(III) reduction. *Geochim. Cosmochim. Acta* **67**, 2735–2748 (2003).

13. Schwertmann, U. & Cornell, R. M. *Iron Oxides in the Laboratory: Preparation and Characterization* (Wiley-VCH, 2000).

14. Steckhan, E. & Kuwana, T. Spectroelectrochemical study of mediators I. Bipyridylium salts and their electron transfer rates to cytochrome c. *Ber. Bunsenges. Phys. Chem.* **78**, 253–259 (1974).

15. Glasser, N. R., Saunders, S. H. & Newman, D. K. The colorful world of extracellular electron shuttles. *Annu. Rev. Microbiol.* **71**, 731–751 (2017).

16. Zarzycki, P., Kerisit, S. & Rosso, K. M. Molecular Dynamics Study of Fe(II) Adsorption, Electron Exchange, and Mobility at Goethite (α-FeOOH) Surfaces. *J. Phys. Chem. C* **119**, 3111–3123 (2015).

17. Wang, D., Crowe, W. E., Strongin, R. M. & Sibrian-Vazquez, M. Exploring the pH dependence of viologen reduction by α-carbon radicals derived from Hcy and Cys. *Chem. Comm.* **60**, 1876–1878 (2009).

18. Lambrev, P. Toolbox for analysis of spectroscopy data, version 2.0.0.0. http://www.mathworks.com/matlabcentral/fileexchange/32828-spectr-o-matic/content/peakdet.m (2017).

19. Gorski, C. A., Edwards, R., Sander, M., Hofstetter, T. B. & Stewart, S. M. Thermodynamic characterization of iron oxide-aqueous Fe^{2+} redox couples. *Environ. Sci. Technol.* **50**, 8538–8547 (2016).

20. Clark, W. M. *Oxidation Reduction Potentials of Organic Systems*, vol. 64 (The Williams and Wilkins Company, Baltimore, MD, 1960).

21. Rosso, K. M., Smith, D. M. A., Wang, Z., Ainsworth, C. C. & Fredrickson, J. K. Self-Exchange Electron Transfer Kinetics and Reduction Potentials for Anthraquinone Disulfonate. *The Journal of Physical Chemistry A* **108**, 3292 – 3303 (2004-04). URL https://pubs.acs.org/doi/abs/10.1021/jp037134u.

22. Dawson, R. M. C., Elliott, W. H. & Elliott, D. C. *Data for Biochemical Research* (Oxford University Press, New York, 1960).

23. Fultz, M. L. & Durst, R. A. Mediator compounds for the electrochemical study of biological redox systems: A compilation. *Anal. Chim. Acta* **140**, 1–18 (1982).

24. Aeschbacher, M., Vergari, D., Schwarzenbach, R. P. & Sander, M. Electrochemical analysis of proton and electron transfer equilibria of the reducible moieties in humic acids. *Environ. Sci. Technol.* **45**, 8385–8394 (2011).

25. Warren, J. J., Tronic, T. A. & Mayer, J. M. The Thermochemistry of Proton-Coupled Electron Transfer Reagents and its Implications. *Chemical Reviews* **110**, 6961–7001 (2010).